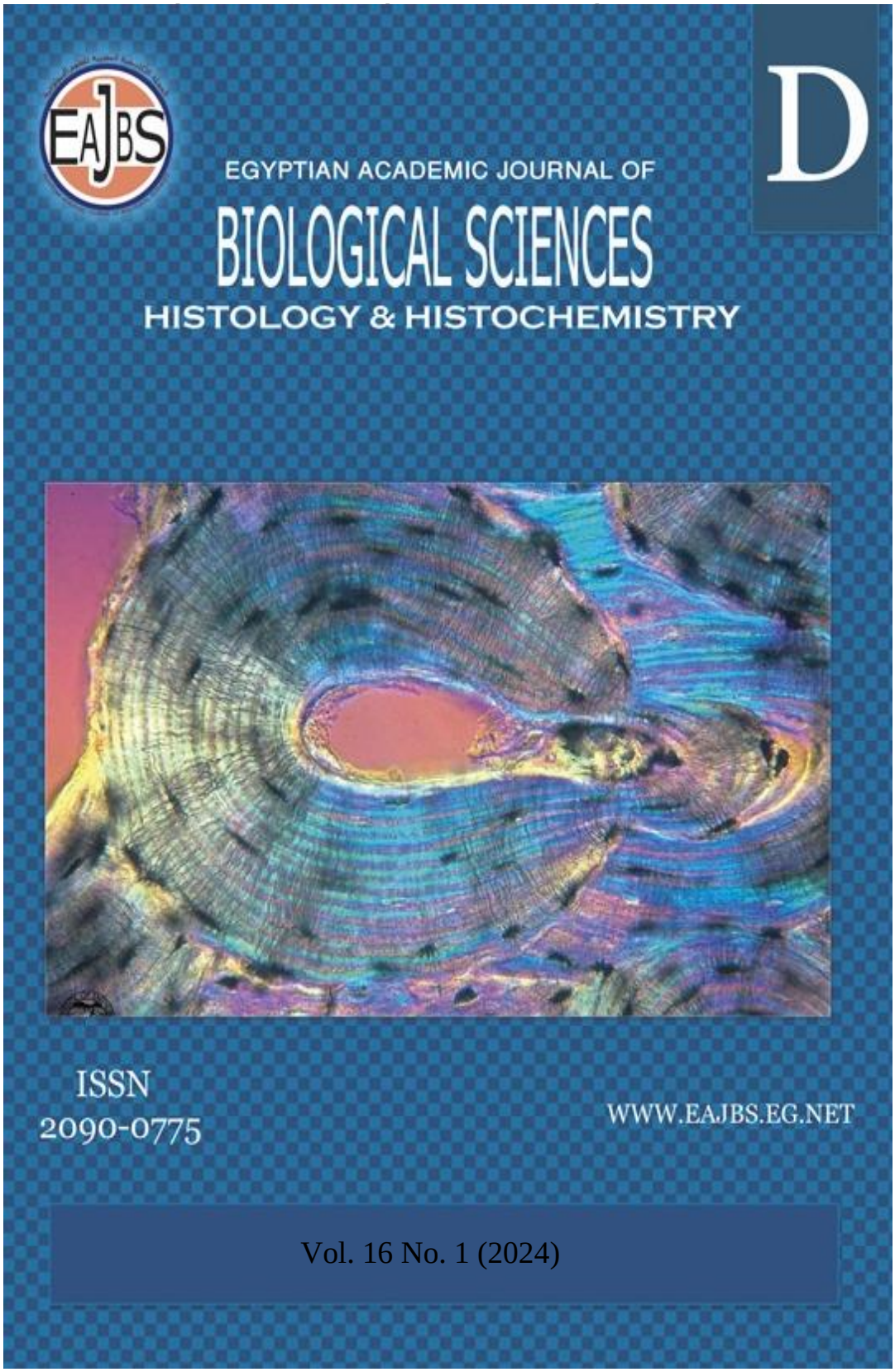

Citation: Egypt. *Acad. J. Biolog. Sci. (D-Histology and histochemistry) Vol.16(1) pp195-216(2024)*
DOI: 10.21608/EAJBSD.2024.361986

Egypt. Acad. J. Biolog. Sci., 16(1): 195-216 (2024)

Egyptian Academic Journal of Biological Sciences
D. Histology & Histochemistry
ISSN 2090 – 0775
http://eajbsd.journals.ekb.eg

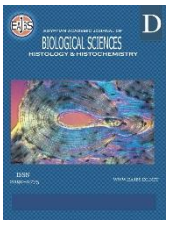

Potential Role of Bone Marrow Mesenchymal Stem Cells in Ameliorating Hippocampal Structural Changes Induced by Aluminium Chloride in Adult Male Albino Rats

Mohamed N. Mahmoud; Dorreia A. Mohamed; Esraa K. Mohamed and Reneah R. Bushra

Human Anatomy and Embryology Department, Faculty of Medicine, Assiut University, Assiut, Egypt

***E-mail:** nabil44mm40@yahoo.com ; reneah@aun.edu.eg

ARTICLE INFO

Article History
Received:23/5/2024
Accepted:26/6/2024
Available:29/6/2024

***Keywords*:**
Hippocampus; Aluminium Chloride; BM-MSCs; Albino Rats.

ABSTRACT

Background: The hippocampus plays a major role in memory. Aluminium chloride ($AlCl_3$) is an Alzheimerogenic compound. Stem cells are promising. **The work aimed to** evaluate the stem cells in ameliorating the hippocampal changes induced by $AlCl_3$. **Material and methods:** 24 adult male albino rats, aged two months, weighing 200-250 gm were randomly divided into group A (control group) that was divided into group A1 (6 rats) received no treatment and group A2 (6 rats) received 1 ml of normal saline intraperitoneally once daily for 60 days, group B ($AlCl_3$-treated group) consisted of 6 rats and received 40 mg $AlCl_3$/kg b.w. intraperitoneally once daily for 60 days, and group C ($AlCl_3$+ MSCs-treated group) consisted of 6 rats and received 40 mg $AlCl_3$/kg b.w. intraperitoneally once daily for 60 days then received an intraperitoneal injection of one million bone marrow mesenchymal stem cells (BM-MSCs) and kept for 3 weeks without treatment. At the designated time, all rats were anaesthetized, sacrificed and the brains were extracted and processed for histological, immunohistochemical, and morphometric studies. **Results:** The hippocampus of group B showed apoptotic cells, vacuolated cytoplasm, eosinophilic patches, neurofibrillary tangles, and dilated congested blood vessels as well as statistically significant decreases in the granular layer and stratum pyramidale thickness, diameter of pyramidal cells' nuclei, and number of pyramidal cells, and an increase of the area % of GFAP, caspase-3 and ubiquitin immunoreactivity. Group C showed a noticeable regression of these changes. **Conclusion:** $AlCl_3$ has an injurious impact on the hippocampus. It could be alleviated by BM-MSCs.

INTRODUCTION

The hippocampus is the flash drive of the human brain. It is vital for learning, memory, and spatial navigation. Connections between the hippocampus and neocortex are important for awareness of conscious knowledge (Mazher & Hassan, 2020). The hippocampus is a convex elevation of grey matter within the parahippocampal gyrus inside the inferior temporal horn of the lateral ventricle. It has three distinct zones of grey matter: the dentate gyrus, Cornu Ammonis (the hippocampus proper), and the subiculum (Dubois *et al.*, 2016).

The hippocampus is the earliest and the most severely affected structure in several neuropsychiatric disorders such as Alzheimer's disease (AD) (Song *et al.,* 2018). AD is accompanied by early dysfunction and loss of synapses, prominently affecting excitatory transmission in the hippocampus and cerebral cortex. These changes may contribute to memory loss because of neuronal loss, specifically glutamatergic neurons of the pyramidal layer of the CA1 sector of the hippocampus (Dudek *et al.,* 2016 and Ali *et al.,* 2022). Although the exact pathology of AD remains unclear, pathologic hallmarks include amyloid-β plaques and neurofibrillary tangles (Song *et al.,* 2018; Mahdi *et al.*, 2019; Sandip & Yogesh, 2019 and Cosacak *et al.,* 2020). The amyloid deposits are believed to originate from the destruction of membrane proteins (Tietz *et al.,* 2019).

Among the commonly used Alzheimerogenic chemicals, heavy metals such as aluminium have been identified to induce toxicity following long-term exposure in humans (Mahdi *et al.,* 2019 and Ali *et al.,* 2022). Aluminium chloride ($AlCl_3$) is the water-soluble form of aluminium found in a solution in combination with other ions and its uptake can take place through food, breathing, and skin contact (Tietz *et al.,* 2019).

Therapeutic trials for AD are palliative and tend to decrease the production of amyloid material or increase its clearance. However, these drugs do not affect disease progression (Song *et al.,* 2018 and Cosacak *et al.,* 2020). Emphasising the neurogenesis aspect can be a potential intervention step toward treatment (Kizil & Bhattarai; 2018 and Choi & Tanzi, 2019).

Transplantation of stem cells has been documented to achieve positive effects in some neurological disease models (Song *et al.,* 2018; Mariacruz, 2019; Han *et al.,* 2019A and Zhang *et al.,* 2019). Mesenchymal stem cells have been identified within different tissues, such as bone marrow, adipose tissue, and umbilical cord (Elwakeel & Mohamed, 2018 and Han *et al.,* 2019A). They are progenitor cells that can differentiate into a variety of cell types from all three germ layers (Song *et al.,* 2018). This ability allows the generation of neural cells (Garcia-Leon *et al.,* 2019). Bone marrow mesenchymal stem cells (BM-MSCs) are known to be easily isolated and expanded with no risk of rejection. Moreover, they have low immunogenicity and therefore the probability of being tumorigenic is even low (Goodarzi *et al.* 2015; Gugliandolo *et al.,* 2017 and Andrzejewska *et al.,* 2019).

Hence, the present work was designed to evaluate the BM-MSCs in ameliorating the hippocampal changes induced by $AlCl_3$.

MATERIAL AND METHODS

Chemicals:

$AlCl_3$ (CAS Number: 7446-70-0; Sigma-Aldrich, St. Louis, MO, USA) in a white powder form, was obtained by El-Gomhouria Company for Trading Chemicals and Medical Appliances.

Isolation and Expansion of BM-MSCs:

BM-MSCs were isolated and expanded from the femurs and tibiae of healthy male albino rats, according to Abo-Azizaa *et al.* (2019) and Mahmoud *et al.* (2024) at the Tissue Culture and Molecular Biology Centre at Assiut University. Using the inverted microscope, BM-MSCs were identified by their typical fibroblast-like spindle shape containing rounded nuclei [Fig. 1].

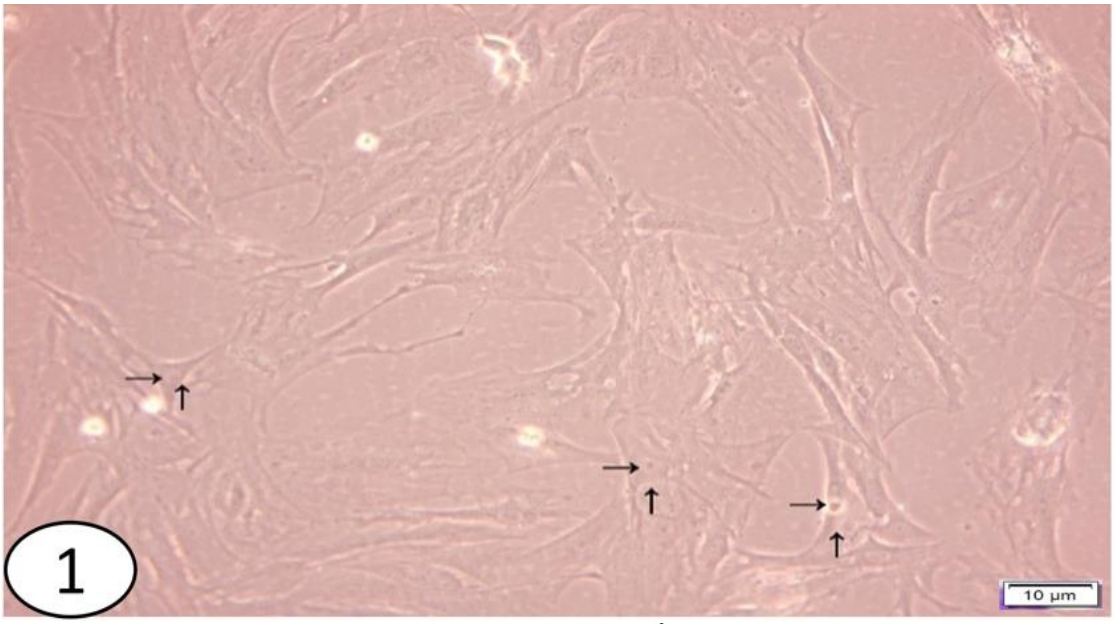

Fig. 1: A photomicrograph of BM-MSCs on the 10th day of culture showing colonies of typical fibroblast-like spindle-shaped stem cells (↑) with rounded nuclei (→). **[X1000]**

Animals and Experimental Design:

A total of 24 adult male albino rats (aged 2 months and weighing 200-250 gm) were gained from the Animal House, Faculty of Medicine, Assiut University. The rats were housed under hygienic conditions in metal cages with 12:12 hours of light: dark cycle. Food and water were available ad libitum. The rats were randomly divided into:

Group A (control group): consisted of 12 rats and was divided into groups A1 and A2. Group A1 (6 rats): received no treatment. Group A2 (6 rats): received 1 ml of normal saline (0.9% NaCl) intraperitoneally once daily for 60 days.

Group B ($AlCl_3$-treated group): consisted of 6 rats and received 40 mg $AlCl_3$/kg b.w.-dissolved in normal saline- intraperitoneally once daily for 60 days (Saba *et al.*, 2017).

Group C ($AlCl_3$+MSCs-treated group): consisted of 6 rats and received 40 mg $AlCl_3$/kg b.w. -dissolved in normal saline- intraperitoneally once daily for 60 days, then received an intraperitoneal injection of a flask of one million BM-MSCs diluted with 1 ml saline and loaded in a sterile syringe. Then they were kept for 3 weeks under normal conditions without any treatment. (Marzban *et al.*, 2018 and Abo-Azizaa *et al.*, 2019).

At the designated time, all animals were anaesthetized with ether inhalation, sacrificed and perfused in the left ventricle by normal saline injection. The brains were extracted and processed for histological, immunohistochemical and morphometrical studies. All procedures of handling, housing and care of the rats were carried out in firm accordance with the ethics approved by the International Guidelines for the Care and Use of Laboratory Animals.

1- Histological Study:

Some brain specimens were fixed in 10% buffered formalin solution. Paraffin blocks were cut serially in coronal planes of 8-10µm thickness, and the slides were stained with haematoxylin and eosin stain (H&E) and gallocyanin and examined with the light microscope.

Other brain specimens were fixed in 2.5% glutaraldehyde + 4% formaldehyde. Semithin sections were stained with toluidine blue and ultrathin sections (60-90 nm thick) were stained with uranyl acetate and lead citrate. The semithin sections were examined with a light microscope. The ultrathin sections were examined with the transmission electron microscope (TEM) ("Jeol"

E.M.-100 CX11; Japan) at the Electron Microscopic Unit of Assiut University.

2- Immunohistochemical Study:

Immunohistochemical detection of GFAP, caspase-3 and ubiquitin of the dentate gyrus and CA1 subfield of the hippocampus was performed using primary mouse anti-GFAP antibody and primary rabbit anti-rat caspase-3 antibody and monoclonal anti-ubiquitin antibody respectively. Immunostaining was performed using avidin-biotin peroxidase, according to Cattoretti *et al.* (1993).

3- Morphometric Study and Statistical Analysis:

The images were analyzed using Image J software to measure the granular cell layer and stratum pyramidale thickness, the diameter of pyramidal cells' nuclei, and the number of pyramidal cells per area of 9540 um^2. Area % of the GFAP, caspase-3 and ubiquitin immunoreactivity of the dentate gyrus and CA1 subfield of the hippocampus were also detected. SPSS software (IBM SPSS Statistics V21.0 Inc., Chicago, Illinois, USA) was used for the statistical analysis. The data were represented as mean ± standard deviation (SD). One-way analysis of variance (ANOVA) followed by the post hoc Tukey test was used to compare the means. P-value < 0.05 was considered statistically significant.

RESULTS

I. Morphological Results:

Group B ($AlCl_3$-treated group) revealed a statistically significant decrease in the granular cell layer and stratum pyramidale thickness, the diameter of pyramidal cells' nuclei, and the number of pyramidal cells per area in comparison to the control. There was no statistically significant difference in group C ($AlCl_3$+ MSCs-treated group) in comparison to the control (Table 1, Histogram 1). On the other hand, the area % of the GFAP, caspase-3 and ubiquitin immunoreactivity of the dentate gyrus and CA1 subfield of the hippocampus exhibited a statistically significant increase in the $AlCl_3$-treated group in comparison to the control. There was no statistically significant difference in the $AlCl_3$+MSCs-treated group in comparison to the control (Tables 2&3, Histograms 2&3).

Table 1: The granular cell layer and stratum pyramidale thickness, the diameter of pyramidal cells' nuclei, and the number of pyramidal cells per area of 9540 um^2 of the studied groups

	Group A mean ± SD	**Group B mean ± SD**	**Group C mean ± SD**	**P-value**
Granular cell layer thickness (µm)	40.2±0.83	25.33±0.88***	38.36±0.49	0.000
Stratum pyramidale thickness (µm)	35.67±0.93	18.91±1.28***	33.83±0.75	0.000
Diameter of pyramidal cells' nuclei (µm)	10.73±0.21	8.98±0.58**	10.2±0.24	0.001
Number of pyramidal cells/area	42±1.41	24±1.78***	40±0.89	0.000

***Differences at $p < 0.001$ in comparison to the control.

**Differences at $p < 0.01$ in comparison to the control.

Table 2: The area % of the GFAP, caspase-3 and ubiquitin immunoreactivity of the dentate gyrus of the studied groups

	Group A mean ± SD	**Group B mean ± SD**	**Group C mean ± SD**	**P-value**
Area % of GFAP immunoreactivity	0.3±0.02	4.16±0.10***	0.39±0.02	0.000
Area % of caspase-3 immunoreactivity	0.66±0.01	16.32±0.40***	0.7±0.05	0.000
Area % of ubiquitin immunoreactivity	1.58±0.37	11.86±0.70***	1.76±0.38	0.000

***Differences at $p < 0.001$ in comparison to the control

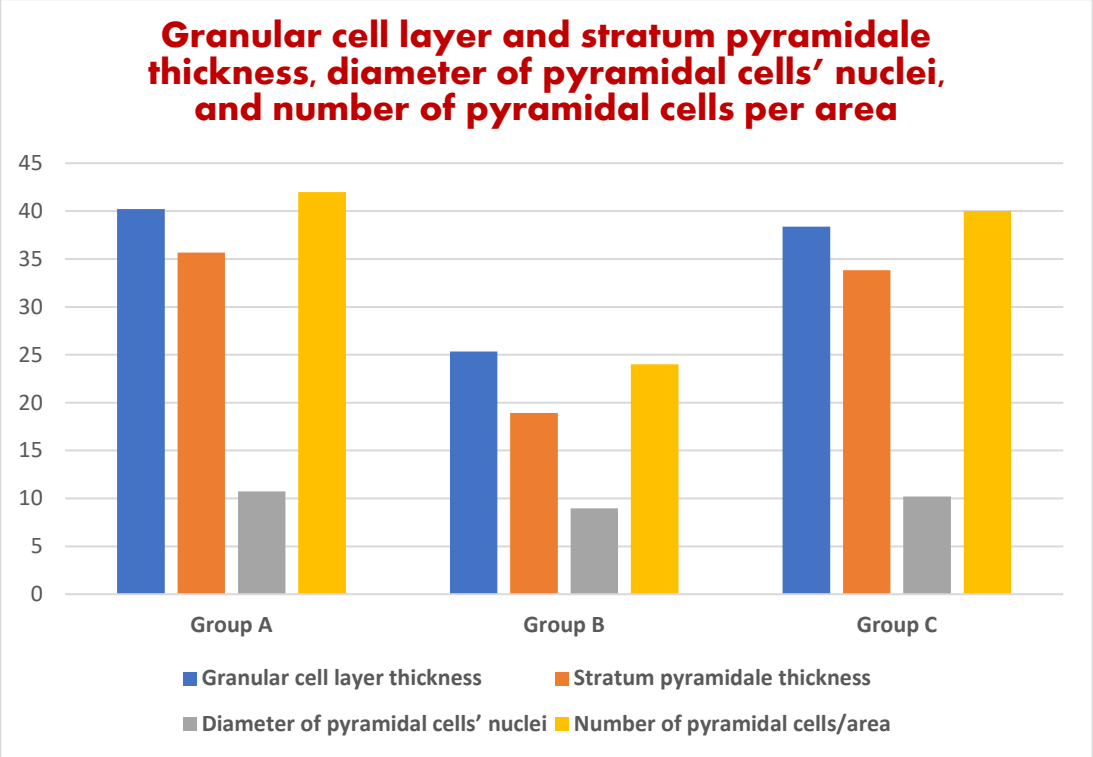

Histogram 1: The granular cell layer and stratum pyramidale thickness, the diameter of pyramidal cells' nuclei, and the number of pyramidal cells per area of 9540 μm^2 of the studied groups.

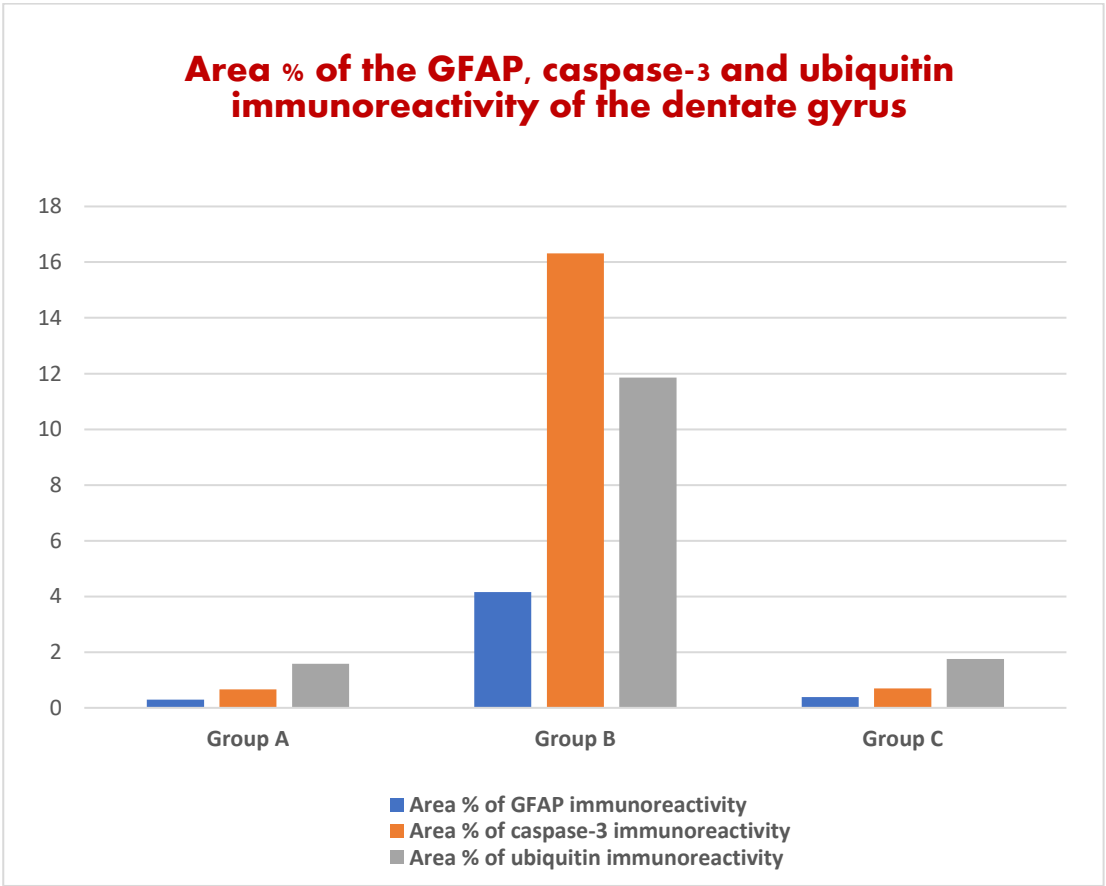

Histogram 2: The area % of the GFAP, caspase-3 and ubiquitin immunoreactivity of the dentate gyrus of the studied groups.

Table 3: The area % of the GFAP, caspase-3 and ubiquitin immunoreactivity of the CA1 subfield of the hippocampus of the studied groups

	Group A mean ± SD	Group B mean ± SD	Group C mean ± SD	P-value
Area % of GFAP immunoreactivity	0.35±0.01	7.62±0.16***	0.38±0.01	0.000
Area % of caspase-3 immunoreactivity	1.62±0.08	12.33±0.58***	1.75±0.11	0.000
Area % of ubiquitin immunoreactivity	4.12±0.23	12.95±0.29***	4.44±0.32	0.000

***Differences at $p < 0.001$ in comparison to the control.

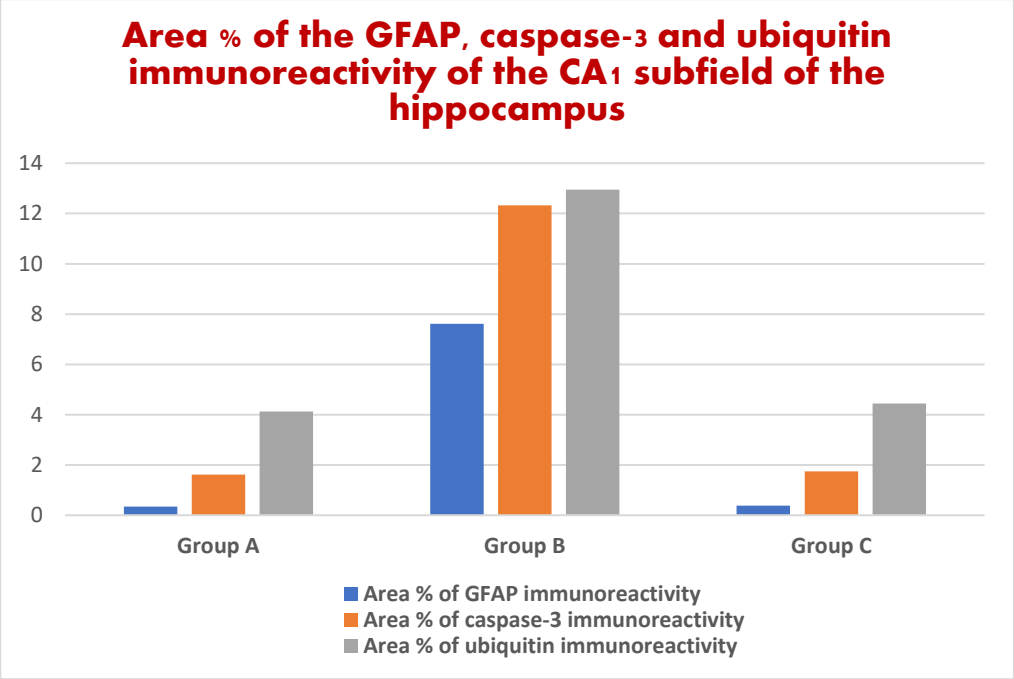

Histogram 3: The area % of the GFAP, caspase-3 and ubiquitin immunoreactivity of the CA1 subfield of the hippocampus of the studied groups.

II-Histological Results:

There was no obvious histological difference between the control groups (group A1 and group A2) throughout the experiment.

1-Light Microscopic Results:

1.1.H&E Stain:

The hippocampus of the control group (group A) was formed of the hippocampus proper and the dentate gyrus. They looked like two interlocking "Cs" being separated by the hippocampal sulcus. The hippocampus proper consisted of strata alveolus, oriens, pyramidale, radiatum and lacunosum-moleculare. Its subfields were CA1, CA2, CA3 and CA4, and it continued as a subiculum. The overlying brain architecture was normal. The dentate gyrus surrounded CA4 by its upper and lower blades and was formed of superficial molecular, middle granular, and deep polymorphic layers. The granular cell layer was formed of small densely packed rounded granule cells containing rounded nuclei and arranged in a laminated manner. Dispersed mossy cells, interneurons and microglial cells with darkly stained nuclei surrounded by lightly stained cytoplasm were noticed [Figs. 2a, 3a, 3d]. The CA1 subfield of the hippocampus revealed strata oriens, pyramidale and radiatum. The stratum pyramidale consisted of pyramidal neurons with rounded nuclei, prominent nucleoli and prominent apical dendrites projecting towards the stratum radiatum. Interneurons were detected within strata oriens and radiatum. Oligodendrocytes, with typical characteristic fried egg appearance, containing small dark round nuclei surrounded by a clear cytoplasm were noticed. Intact blood vessels were observed [Figs. 4a, 4d].

The $AlCl_3$-treated group (group B) revealed a dilated hippocampal sulcus. Vacuoles were noticed in the overlying brain architecture. Scattered eosinophilic patches were observed in the hippocampus as well as in the overlying brain tissue. The dentate gyrus exhibited vacuoles, apoptotic neurons, ballooning of granule cells, pyknotic cells with eosinophilic cytoplasm, microglial cells, astrocytes, and degenerated mossy cells [Figs. 2b, 3b, 3e]. The CA1 subfield of the hippocampus showed pyramidal neurons with eosinophilic cytoplasm, apoptotic and pyknotic nuclei, less prominent apical dendrites, pericellular haloes, neurofibrillary tangles, and dilated congested blood vessels. Some pyramidal cells with rounded nuclei were observed [Figs. 4b, 4e].

The $AlCl_3$+MSCs-treated group (group C) showed nearly normal CA1, CA2, CA3 and CA4 subfields of the hippocampus proper, hippocampal sulcus, subiculum, overlying brain architecture, strata alveolus, oriens, pyramidale, radiatum and lacunosum moleculare, upper and lower blades of the dentate gyrus and molecular, granular and polymorphic layers. Granule cells with rounded nuclei and prominent nucleoli, interneurons, dividing microglial cells, residual vacuoles, and degenerated mossy cells were noticed [Figs. 2c, 3c, 3f]. The CA1 subfield of the hippocampus showed strata oriens, pyramidale and radiatum, pyramidal neurons with rounded nuclei, prominent nucleoli and apical dendrites, blood vessels, and oligodendrocytes with fried egg appearance [Figs. 4c, 4f].

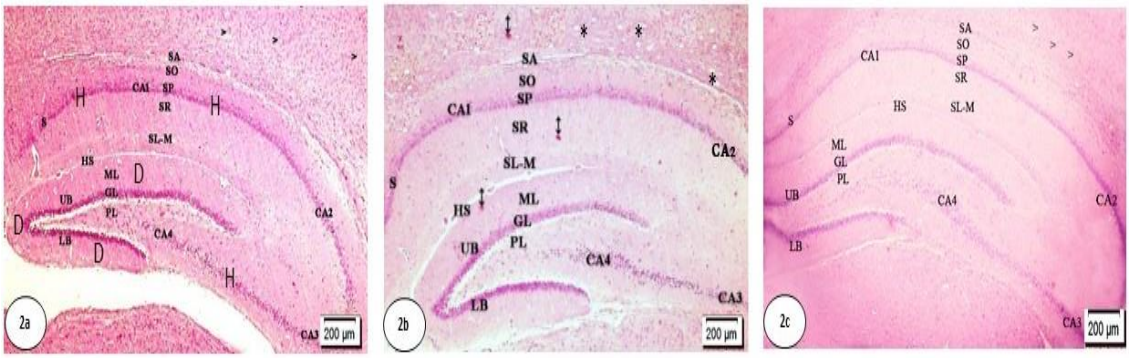

Fig. 2: Photomicrographs of coronal sections of the hippocampus of the examined groups. The control group shows the hippocampal sulcus (HS) separating the 2 interlocking C-shaped hippocampus proper (H) and dentate gyrus (D). (CA1), (CA2), (CA3) and (CA4) subfields of the hippocampus proper, subiculum (S) and strata alveolus (SA), oriens (SO), pyramidale (SP), radiatum (SR) and lacunosum moleculare (SL-M) are well-defined. The upper (UB) and lower (LB) blades of the dentate gyrus surround the CA4 subfield. The dentate gyrus is formed of superficial molecular (ML), middle granular (GL), and deep polymorphic (PL) layers. Note the normal overlying brain architecture (>) **[Fig. 2a]**. The $AlCl_3$-treated group shows (CA1), (CA2), (CA3), and (CA4) subfields of the hippocampus proper, subiculum (S), strata alveolus (SA), oriens (SO), pyramidale (SP), radiatum (SR) and lacunosum moleculare (SL-M), upper (UB) and lower (LB) blades of the dentate gyrus, and molecular (ML), granular (GL) and polymorphic (PL) layers. Notice the dilated hippocampal sulcus (HS), vacuoles (*) and scattered eosinophilic patches (↕) **[Fig. 2b]**. The $AlCl_3$+ MSCs-treated group shows nearly normal (CA1), (CA2), (CA3) and (CA4) subfields of the hippocampus proper, hippocampal sulcus (HS), subiculum (S), overlying brain architecture (>), strata alveolus (SA), oriens (SO), pyramidale (SP), radiatum (SR) and lacunosum moleculare (SL-M), upper (UB) and lower (LB) blades of the dentate gyrus and molecular (ML), granular (GL) and polymorphic (PL) layers **[Fig. 2c]**. **[H&E; X40]**

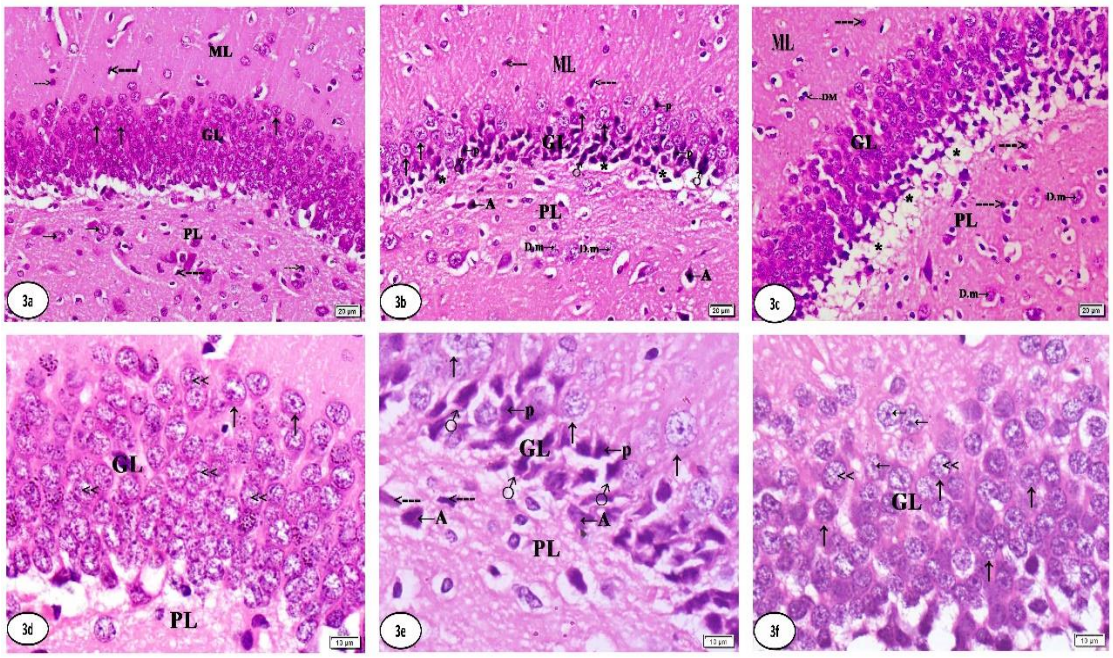

Fig. 3: Photomicrographs of coronal sections of the dentate gyrus of the examined groups. The control group shows molecular (ML), granular (GL) and polymorphic (PL) layers. The granular cell layer (GL) is formed of small densely packed rounded granule cells (↑) containing rounded nuclei (<<) and arranged in a laminated manner. Note the dispersed mossy cells (→), interneurons (--->) and microglial cells with darkly stained nuclei surrounded by lightly stained cytoplasm (<---) **[Figs. 3a, 3d].** The $AlCl_3$-treated group shows molecular (ML), granular (GL), and polymorphic (PL) layers, vacuoles (*), apoptotic neurons (♂), ballooning of granule cells (↑), pyknotic cells with eosinophilic cytoplasm (←p), microglial cells (<---), astrocytes (←A) and degenerated mossy cells (D.m→) **[Figs. 3b, 3e].** The $AlCl_3$+ MSCs-treated group shows molecular (ML), granular (GL) and polymorphic (PL) layers, granule cells (↑) with rounded nuclei (<<) and prominent nucleoli (←), and interneurons (--->). Residual vacuoles (*), dividing microglial cells (<---DM), and degenerated mossy cells (D.m→) are noticed **[Figs. 3c, 3f]. [H&E: Figs. 3a-c→ X400, Figs. 3d-f→X1000, respectively]**

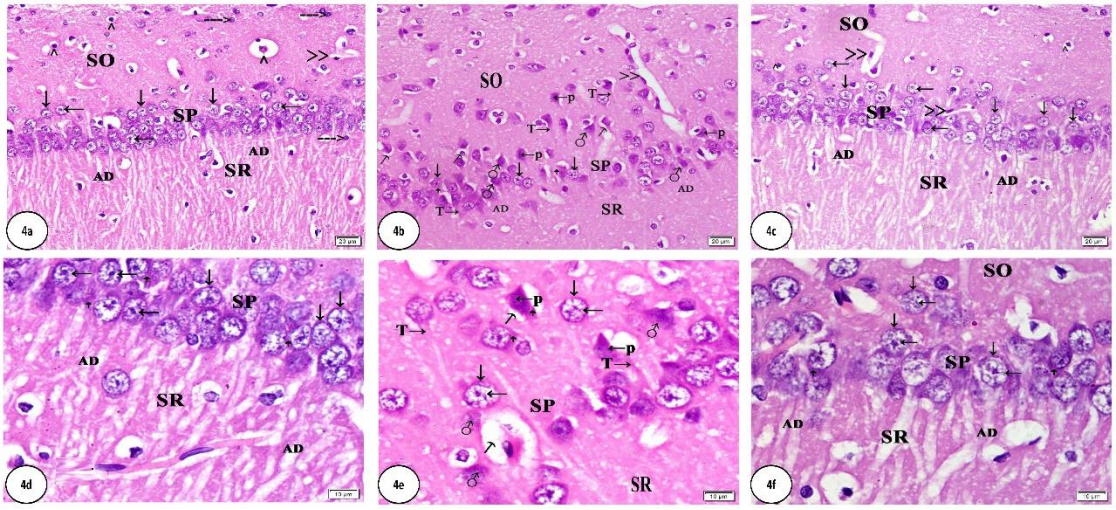

Fig. 4: Photomicrographs of coronal sections of the CA1 subfield of the hippocampus of the examined groups. The control group shows strata oriens (SO), pyramidale (SP) and radiatum (SR). The pyramidal neurons (↓) contain rounded nuclei with prominent nucleoli (←) and apical dendrites (AD) projecting towards the stratum radiatum (SR). Oligodendrocytes (∧) with fried egg appearance, interneurons (--->), and blood vessels (>>) are detected **[Figs. 4a, 4d].** The $AlCl_3$-treated group shows strata oriens (SO), pyramidale (SP) and radiatum (SR). Notice the pyramidal neurons (↓) with eosinophilic cytoplasm (↑), apoptotic (♂) and pyknotic (←p) nuclei, less prominent apical dendrites (AD), pericellular haloes (↗), and neurofibrillary tangles (T→). Dilated congested blood vessels (>>) are seen. Some pyramidal cells with rounded nuclei (←) are observed **[Figs. 4b, 4e].** The $AlCl_3$+ MSCs-treated group shows strata oriens (SO), pyramidale (SP) and radiatum (SR) and pyramidal neurons (↓) with rounded nuclei and prominent nucleoli (←), basophilic cytoplasm (↑) and apical dendrites (AD). Oligodendrocytes (∧) with fried egg appearance and blood vessels (>>) are noticed **[Figs. 4c, 4f]. [H&E: Figs. 4a-c→ X400, Figs. 4d-f→ X1000, respectively]**

1.2. Gallocyanin Stain:

The dentate gyrus of the control group showed molecular, granular, and polymorphic layers. The granular cell layer was formed of small densely packed rounded granule cells with highly basophilic cytoplasm and rounded nuclei with clumped chromatin [Figs. 5a, 5d]. The CA1 subfield showed well-defined strata alveolus, oriens, pyramidale and radiatum. The stratum pyramidale consisted of pyramidal neurons with basophilic cytoplasm and large rounded nuclei. Apical dendrites were projecting towards the stratum radiatum. A few microglial cells with darkly stained nuclei surrounded by lightly stained space, and dispersed interneurons were noted [Figs. 6a, 6d].

The $AlCl_3$-treated group showed ballooning of granule cells, apoptotic cells, less basophilic cytoplasm of most granule cells than control, pyknotic nuclei and neurons demonstrating visible neurofibrillary tangles. Intact granule cells with rounded nuclei were noticed. Vacuoles appeared beneath the granular cell layer. The polymorphic layer showed degenerated mossy cells. Dividing microglia appeared within the molecular and polymorphic layers [Figs. 5b, 5e]. The stratum pyramidale showed disarranged pyramidal neurons, visible neurofibrillary tangles, apoptotic pyramidal cells, and less prominent apical dendrites. Pyramidal neurons containing rounded nuclei were observed [Figs. 6b, 6e].

The $AlCl_3$+ MSCs-treated group showed molecular, granular and polymorphic layers, and densely packed rounded granule cells arranged in a laminated manner and containing basophilic cytoplasm. Residual vacuoles beneath the granular cell layer were seen. The neurofibrillary tangles were not

noticed [Figs. 5c, 5f]. The CA1 subfield of the hippocampus demonstrated strata oriens, pyramidale and radiatum. The stratum pyramidale consisted of pyramidal neurons with large and rounded nuclei and basophilic cytoplasm. Apical dendrites projecting towards the stratum radiatum were observed. The neurofibrillary tangles were not noticed [Figs. 6c, 6f].

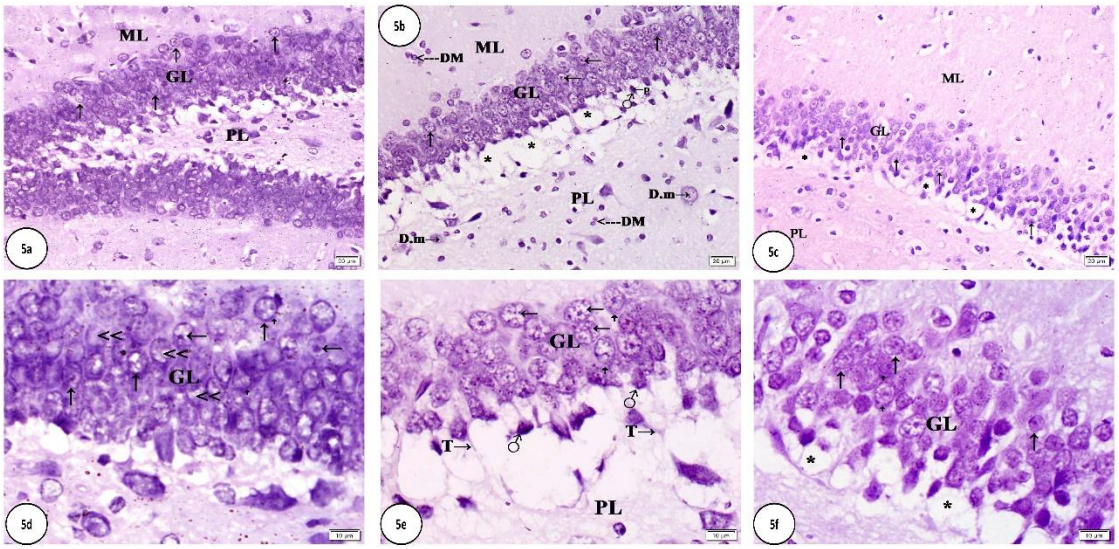

Fig. 5: Photomicrographs of coronal sections of the dentate gyrus of the examined groups. The control group shows molecular (ML), granular (GL) and polymorphic (PL) layers. The granular cell layer (GL) is formed of small densely packed rounded granule cells (↑) with highly basophilic cytoplasm (↑) and rounded nuclei (←) with clumped chromatin (<<) **[Figs. 5a, 5d].** The $AlCl_3$-treated group shows ballooning of granule cells (↑), apoptotic cells (♂), less basophilic cytoplasm (↑), pyknotic nuclei (←p) and neurofibrillary tangles (T→). Intact granule cells with rounded nuclei **(←)** are noticed. Vacuoles (*) appear beneath the granular cell layer (GL). The polymorphic layer (PL) shows degenerated mossy cells (D.m→). Dividing microglia **(<---DM)** appear within the molecular layer (ML) as well as the polymorphic layer (PL) **[Figs. 5b, 5e].** The $AlCl_3$+ MSCs-treated group shows molecular (ML), granular (GL) and polymorphic (PL) layers, densely packed rounded granule cells arranged in a laminated manner (↑) and containing basophilic cytoplasm (↑), and residual vacuoles (*) beneath the granular cell layer (GL). Note the absence of the neurofibrillary tangles **[Figs. 5c, 5f]. [Gallocyanin stain: Figs. 5a-c; X400, Figs. 5d-f; X1000, respectively]**

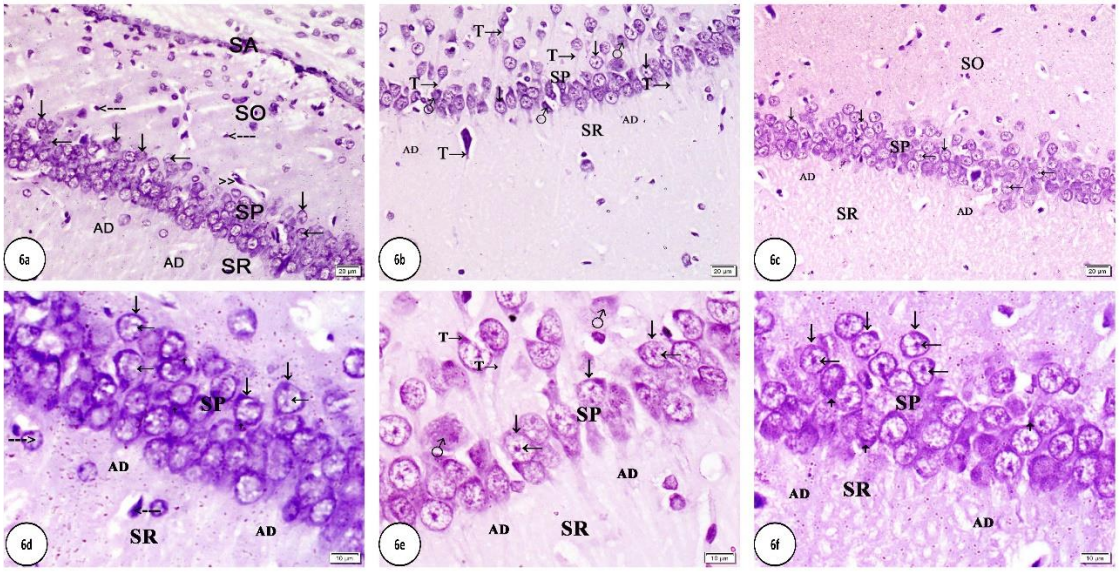

Fig. 6: Photomicrographs of coronal sections of the CA1 subfield of the hippocampus of the examined groups. The control group shows well-defined strata alveolus (SA), oriens (SO), pyramidale (SP) and radiatum (SR), pyramidal neurons (↓) with basophilic cytoplasm (↑), rounded nuclei (←) and apical dendrites (AD) projecting towards the stratum radiatum, microglial cells (<---) with darkly stained nuclei surrounded by lightly stained space, and interneurons (--->) **[Figs. 6a, 6d].** The $AlCl_3$-treated group shows disarrangement of the pyramidal neurons (↓) of the stratum pyramidale (SP), apoptotic pyramidal cells (♂), less prominent apical dendrites (AD) projecting towards the stratum radiatum (SR), and neurofibrillary tangles (T→). Some pyramidal neurons with rounded nuclei (←) are noticed [**Figs. 6b, 56].** The $AlCl_3$+ MSCs-treated group shows strata oriens (SO), pyramidale (SP) and radiatum (SR). Normal pyramidal neurons (↓) with rounded nuclei (←), basophilic cytoplasm (↑), and apical dendrites (AD) were observed. Notice the absence of the neurofibrillary tangles **[Figs. 6c, 6f]. [Gallocyanin stain: Figs. 6a-c; X400, Figs. 6d-f; X1000, respectively]**

1.3. Toluidine Blue Stain:

The control group showed molecular, granular and polymorphic layers, granular cells with rounded nuclei and prominent nucleoli [Fig. 7a], strata oriens, pyramidale, and radiatum, and pyramidal neurons with rounded nuclei and apical dendrites [Fig. 7d].

The AlCl3-treated group showed a noticeable decreased granular cell layer thickness, apoptotic cells, vacuolization, degenerated mossy cells, and linear neurofibrillary tangle. Some intact granule cells with rounded nuclei were observed [Fig. 7b]. The CA1 subfield of the hippocampus showed decreased stratum pyramidale thickness, apoptotic pyramidal cells, less prominent apical dendrites, and linear dark plaques [Fig. 7e].

The AlCl3+ MSCs-treated group retained the thickness of the granular cell layer. Densely packed small granular cells were arranged in a laminated manner. The stratum pyramidale showed an improvement in its thickness. Apical dendrites of pyramidal neurons were prominent and projecting towards the stratum radiatum [Figs. 7c, 7f].

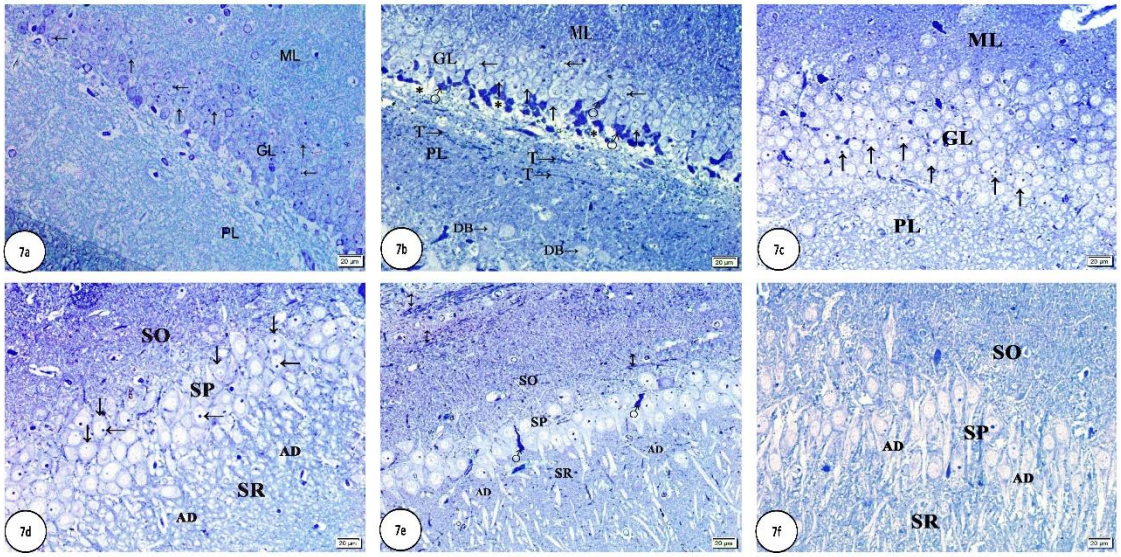

Fig. 7: Photomicrographs of coronal sections of the dentate gyrus **[Figs. 7a-c]** and CA1 subfield of the hippocampus **[Figs. 7d-f]** of the examined groups. The control group shows molecular (ML), granular (GL) and polymorphic (PL) layers, granular cells **(**↑) with rounded nuclei and prominent nucleoli (←) **[Fig. 7a]**, strata oriens (SO), pyramidale (SP), and radiatum (SR), and pyramidal neurons (↓) with rounded nuclei (←) and apical dendrites (AD) **[Fig. 7d].** The $AlCl_3$-treated shows decreased granular cell layer thickness (GL), adjacent molecular (ML) and polymorphic (PL) layers, apoptotic cells (♂), vacuolization (*), degenerated mossy cells (DB→), linear neurofibrillary tangle (T→), intact granule cells (↑) with rounded nuclei (←) **[Fig. 7b]**, decreased stratum pyramidale thickness (SP), adjacent strata oriens (SO), and radiatum (SR), apoptotic pyramidal cells (♂), less prominent apical dendrites (AD), and linear dark plaques (↕) **[Fig. 7e].** The $AlCl_3$+ MSCs-treated group shows retained granular layer thickness (GL), adjacent molecular (ML) and polymorphic (PL) layers, densely packed small granular cells arranged in a laminated manner (↑) **[Fig. 7c]**, improvement in the thickness of stratum pyramidale (SP), strata oriens (SO) and radiatum (SR), and pyramidal neurons (↓) with rounded nuclei (←) and apical dendrites (AD) **[Fig. 7f]. [Toluidine blue; X400]**

2-Electron Microscopic Results:

The granule cells of the control group showed a regular rounded outline with an intact cell membrane. The nuclei were central, rounded euchromatic with a clear nuclear envelope. The cytoplasm contained numerous mitochondria, rough endoplasmic reticulum, and free ribosomes. Myelinated nerve fibres were recognized [Figs. 8a, 8d]. The pyramidal cells had central, rounded euchromatic nuclei with a clear nuclear envelope and prominent nucleoli, and apical dendrites. The cytoplasm contained numerous mitochondria, rough endoplasmic reticulum, and free ribosomes. Myelinated nerve fibres were observed [Figs. 9a, 9d].

The granule cells of the $AlCl_3$-treated group exhibited shrunken heterochromatic nuclei, vacuolated cytoplasm, swollen mitochondria with distorted cristae, lysosomes, few free ribosomes, and numerous inclusions. Microglial cells were noticed with dense heterochromatin lining the nuclear membrane, a narrow rim of contrasting light cytoplasm and microglial processes. Myelinated nerve fibres, and rounded granule cells' nuclei with nuclear envelope and eccentric nucleoli were also observed [Figs. 8b, 8e]. The pyramidal cells had hypochromatic nuclei, intracellular vacuolization, shrunken and swollen mitochondria, lysosomes and a few free ribosomes. Degenerated demyelinated nerve fibres as well as intact ones were noticed [Figs. 9b, 9e].

The granule cells of the $AlCl_3$+ MSCs-treated group showed regular rounded outlines with intact cell membranes, central rounded euchromatic nuclei with a clear nuclear envelope, mitochondria, free ribosomes, and rough endoplasmic reticulum [Figs. 8c, 8f]. The pyramidal cells had apical dendrites and basally-located rounded euchromatic nuclei with a prominent nucleolus and a clear nuclear envelope. The cytoplasm contained mitochondria, lysosomes, free ribosomes and rough endoplasmic reticulum [Figs. 9c, 9f].

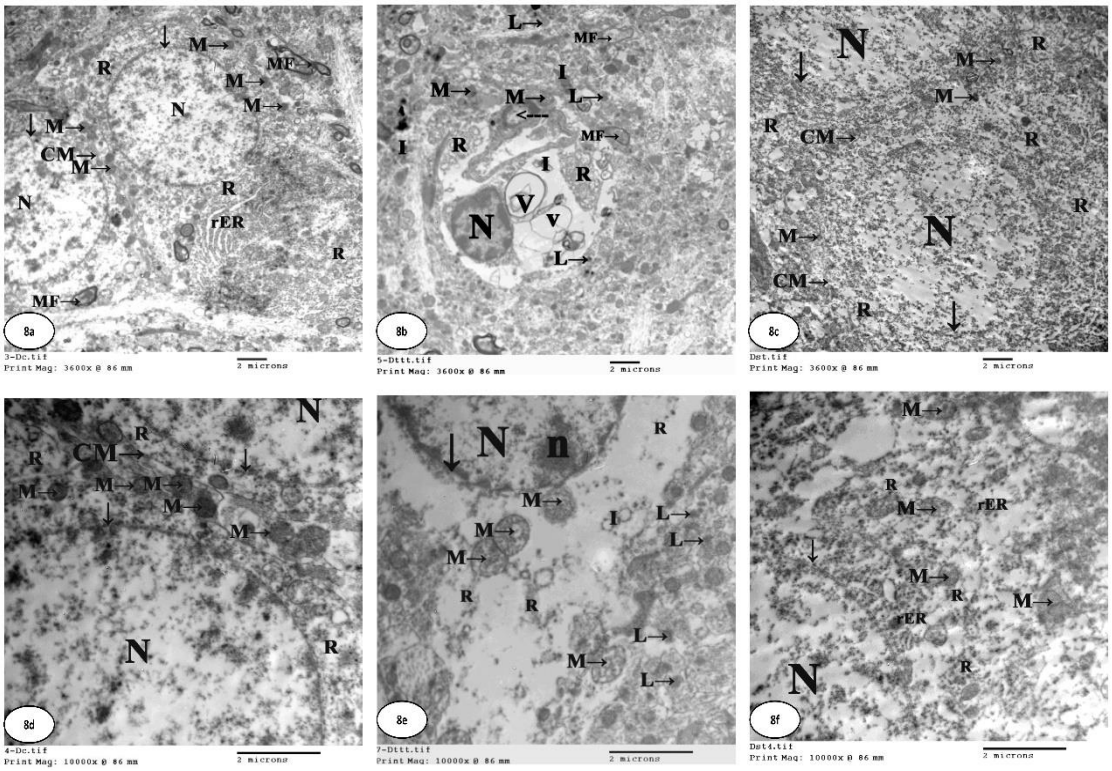

Fig. 8: TEM photomicrographs of the granule cells of the examined groups. A control group shows a regular rounded outline with intact cell membranes (CM→). The nuclei (N) are central rounded euchromatic with clear nuclear envelopes (↓). The cytoplasm contains numerous mitochondria (M→), rough endoplasmic reticulum (rER) and free ribosomes (R). Myelinated nerve fibres are recognized (MF→) **[Figs. 8a, 8d].** The $AlCl_3$-treated group shows a shrunken heterochromatic nucleus (N), vacuolated cytoplasm (V), myelinated nerve fibres (MF→), microglial cells with dense heterochromatin lining the nuclear membrane, a narrow rim of contrasting light cytoplasm and microglial process (<---) **[Fig. 8b],** swollen mitochondria with distorted cristae (M→), lysosomes (L→), few free ribosomes (R), and numerous inclusions (I) **[Figs. 8b, 8e].** A rounded nucleus (N) with eccentric nucleolus (n) and nuclear envelope (↓) is observed **[Fig. 8e].** The $AlCl_3$+ MSCs-treated group shows regular rounded outlines with intact cell membranes (CM→), central rounded euchromatic nuclei (N) with a clear nuclear envelope (↓), mitochondria (M→), free ribosomes (R), and rough endoplasmic reticulum (rER) **[Figs. 8c, 8f]. [TEM: Figs. 8a-c; X 3600, Figs. 8d-f; X 10000, respectively]**

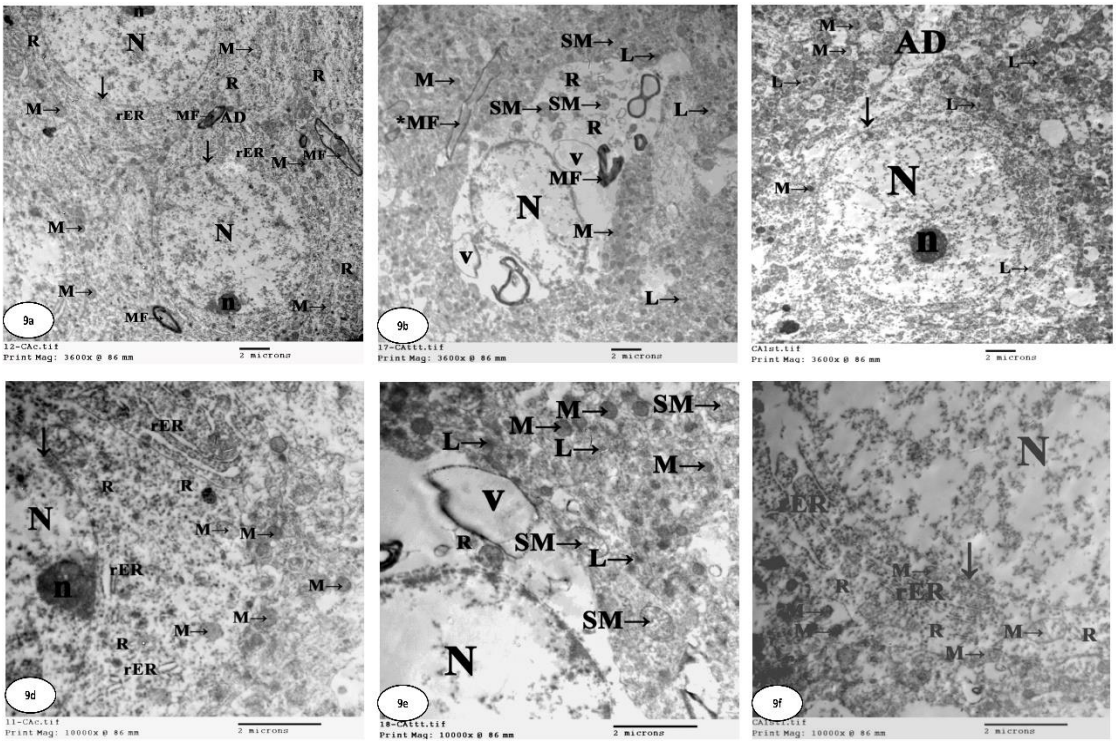

Fig. 9: TEM photomicrographs of the pyramidal cells of the examined groups. The control group shows the cells have central rounded euchromatic nuclei (N) with prominent nucleoli (n) and a clear nuclear envelope (↓) and apical dendrites (AD). The cytoplasm contains numerous mitochondria (M→), rough endoplasmic reticulum (rER), and free ribosomes (R). Myelinated nerve fibres (MF→) are observed **[Figs. 9a, 9d].** The $AlCl_3$-treated group shows hypochromatic nuclei (N), intracellular vacuolization (V), shrunken mitochondria (M→), swollen mitochondria (SM→), lysosomes (L→), and few free ribosomes (R). Degenerated demyelinated nerve fibres (*MF→) and intact myelinated nerve fibres (MF→) are observed **[Figs. 9b, 9e].** The $AlCl_3$+ MSCs-treated group shows an apical dendrite (AD), basal rounded euchromatic nucleus (N) with a prominent nucleolus (n) and a clear nuclear envelope (↓), mitochondria (M→), lysosomes (L→), free ribosomes (R), and rough endoplasmic reticulum (rER) **[Figs. 9c, 9f]. [TEM: Figs. 9a-c; X 3600, Figs. 9d-f; X 10000, respectively]**

3- Immunohistochemical Results:

The dentate gyrus of the control group showed weak positive GFAP, caspase-3, and ubiquitin immunoreactions [Figs. 10a, 10d, 10g]. The CA1 subfield of the hippocampus also revealed weak positive GFAP, caspase-3 and ubiquitin immunoreactions [Figs. 11a, 11d, 11g].

The dentate gyrus of the $AlCl_3$-treated group showed strong positive GFAP, caspase-3, and ubiquitin immunoreactions. Brownish deposits were detected [Figs. 10b, 10e, 10h]. The CA1 subfield of the hippocampus also revealed strong positive GFAP, caspase-3 and ubiquitin immunoreactions. GFAP-stained hypertrophied astrocytes and brownish deposits were detected [Figs. 11b, 11e, 11h].

The dentate gyrus of the $AlCl_3$+ MSCs-treated group showed moderate positive GFAP, caspase-3, and ubiquitin immunoreactions. Residual brownish deposits were noticed [Figs. 10c, 10f, 10i]. The CA1 subfield of the hippocampus revealed moderate positive GFAP, caspase-3, and ubiquitin immunoreactions. Residual brownish deposits were noticed [Figs. 11c, 11f, 11i].

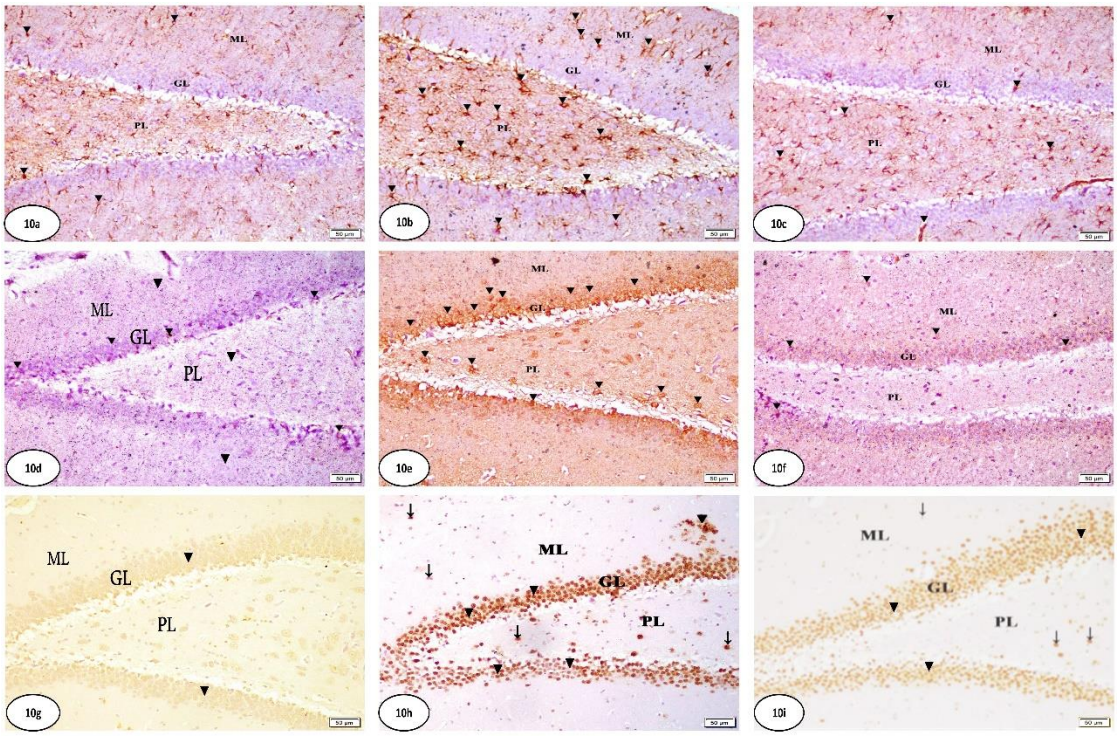

Fig. 10: Photomicrographs of immunohistochemical staining of the dentate gyrus of the examined groups. The control group shows weak positive immunoreactions (▼) within the molecular (ML), granular (GL) and polymorphic (PL) layers **[Figs. 10a, d, g].** The $AlCl_3$-treated group shows strong positive immunoreactions (▼) within the molecular (ML), granular (GL) and polymorphic (PL) layers **[Figs. 10b, e, h].** Notice the brownish deposits (↓) **[Fig. 10h].** The $AlCl_3$+ MSCs-treated group shows moderate positive immunoreactions (▼) within the molecular (ML), granular (GL) and polymorphic (PL) layers **[Figs. 10c, f, i].** Residual brownish deposits (↓) are noticed **[Fig. 10i]. [GFAP immunohistochemical staining → Figs. 10a-c; caspase-3 immunohistochemical staining → Figs. 10d-f; ubiquitin immunohistochemical staining → Figs. 10g-i, respectively; X200]**

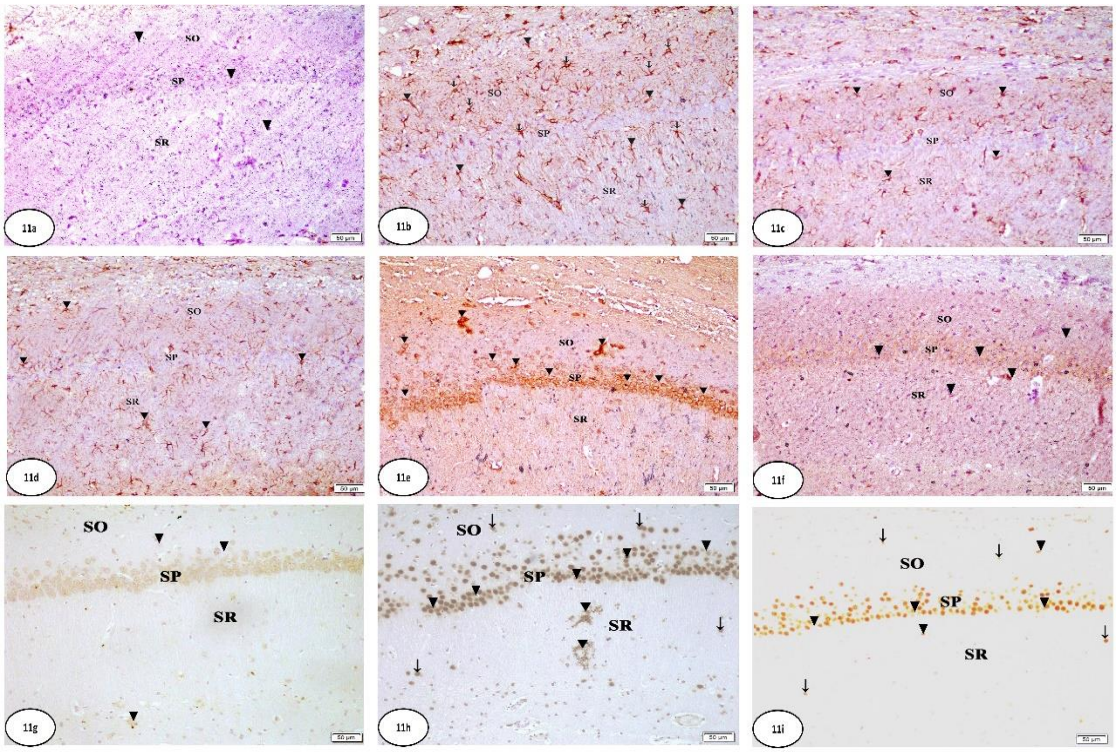

Fig. 11: Photomicrographs of immunohistochemical staining of the CA1 subfield of the hippocampus of the examined groups. The control group shows weak positive immunoreactions (▼) within the strata oriens (SO), pyramidale (SP) and radiatum (SR) **[Figs. 11a, d, g].** The $AlCl_3$-treated group shows strong positive immunoreactions (▼) within the strata oriens (SO), pyramidale (SP) and radiatum (SR) **[Figs. 11b, e, h].** GFAP-stained hypertrophied astrocytes are detected (↓) **[Fig. 11b].** Brownish deposits (↓) are noticed **[Fig. 11h].** The $AlCl_3$+ MSCs-treated group shows moderate positive immunoreactions (▼) within the strata oriens (SO), pyramidale (SP) and radiatum (SR) [**Figs. 11c, f, i].** Residual brownish deposits (↓) are noticed **[Fig. 11i]. [GFAP immunohistochemical staining → Figs. 11a-c; caspase-3 immunohistochemical staining → Figs. 11d-f; ubiquitin immunohistochemical staining → Figs. 11g-i, respectively; X200]**

DISCUSSION

The hippocampus is the earliest and most severely affected structure in AD (Ju & Tam, 2022). The light microscopic results of the current study declared eosinophilic patches as well as visible neurofibrillary tangles scattered among the hippocampal neurons of the $AlCl_3$-treated rats. This finding is the neuropathologic cardinal feature for the diagnosis of AD as reported by Mahdi *et al.* (2019), Lowe *et al.* (2020), Sengoku (2020) and El-Roghy *et al.* (2022). Lowe *et al.* (2020) stated that the eosinophilic patches are amyloid plaques formed by the accumulation of Aβ40 and Aβ42 peptides that result from the abnormal processing of amyloid precursor protein. The imbalance in the production and clearance pathways shares in the deposition of those plaques and even neural tissue atrophy (Sengoku, 2020).Singh *et al.* (2018) and DeTure and Dickson (2019) demonstrated that the neurofibrillary tangles are composed of filamentous tau proteins, and corruption of normal tau is thought to be a potential factor involved in the spreading of tau pathology throughout the brain and correlated with cognitive impairment and neuronal death.

The granular cells of the dentate gyrus and the pyramidal neurons of the CA1 subfield of the $AlCl_3$-treated group contained pyknotic nuclei and the granular cell layer and the stratum pyramidale decreased in thickness. These in general come in line with the studies of Kumar *et al.* (2018) and Singh *et al.* (2018) who described them as

histological hallmarks of degeneration. The hippocampal sulcus was also dilated in the present $AlCl_3$-treated group, and this was in accordance with DeTure and Dickson (2019), who observed a widening of the sulcal spaces and a narrowing of the gyri in AD patients compared to a normal brain. They attributed these findings to the massive loss of neurons through either necrosis or necroptosis.

The present work showed distorted architecture, dilation, and congestion of the blood vessels of the $AlCl_3$-treated group. These might be signs of accompanied vascular angiopathy and come in line with studies of Singh *et al.* (2018) and El-Roghy *et al.* (2022), who declared subsequent vascular congestion followed $AlCl_3$ and added that the cerebral amyloid angiopathy represents a common concurrent pathology in AD that leads to neurodegeneration.

Oxidative stress is considered another possible mechanism for the observed neurodegeneration in the present work of AD as mentioned by Rodríguez-Vera *et al*. (2022). High brain aluminium concentrations are claimed to cause an imbalance between oxidants and antioxidants in favour of the oxidants which ends in cell disruption and molecular damage (Mahdi *et al.,* 2019). The nervous system is particularly sensitive to oxidant-mediated damage because of its high oxygen consumption rate (Kimberley *et al.,* 2017). In addition, the activities of brain antioxidant enzymes (catalase, superoxide dismutase and glutathione peroxidase) are lower than those found in other tissues (Birhane *et al.,* 2015).

The $AlCl_3$-treated group of the present study revealed dividing microglia. This is considered a sign of their activity and comes in line with studies of Dugger and Dickson (2017) and Justin-Thenmozhi *et al.* (2018). Microglia are the brain's immune cells and play a role in phagocytes, recognizing and scavenging dead cells and pathogens (Da Mesquita *et al.,* 2016 and Von Bartheld *et al.,* 2016). Under stress as damage or infection, they can release inflammatory factors and cause neuroinflammatory responses (Liu *et al.,* 2020 and Ali *et al.,* 2022).

The ultrastructural results of the study confirmed the light picture and pointed out the destructed architecture of the granule cells and pyramidal neurons of the hippocampus of $AlCl_3$-treated rats. The lost chromatin material of the nuclei indicated the lack of transcriptional activity, as reported by Cabianca *et al.* (2019). The present work showed vacuolization of the cytoplasm synchronized with the destructed architecture of the cells. These findings are in line with El-Roghy *et al.,* (2022). Beretta *et al.* (2020) stated that the lipophilic bases in neutral extracellular fluid are uncharged and can be transported through the plasma membrane via passive diffusion or active transport. After entering acidic endosomal-lysosomal organelles, they become positively charged and lose the capacity to diffuse through the organelle membranes back to the cytoplasm. With the further accumulation of charged forms of those bases, the intraorganellar osmotic pressure increases, and the disturbed equilibration leads to the formation of the vacuoles that accompany cell death.

As regards the immunohistochemical study, the hippocampus of the $AlCl_3$-treated group of the present work showed a strong positive GFAP immunoreaction. This finding was in agreement with Liddelow *et al.* (2017), Justin-Thenmozhi *et al.* (2018) and Andrzejewska *et al.* (2021) and could be explained by Liddelow *et al.* (2017), who reported that the astrocytes provide trophic support for neurons and synapses normally. After brain pathology, they undergo a pronounced transformation called 'reactive astrocytosis'. Moreover, Justin-Thenmozhi *et al.* (2018) stated that astrocytes lose most of their normal functions and gain a new neurotoxic

function, rapidly killing neurons and mature differentiated oligodendrocytes.

The present work also revealed strong positive caspase-3 immunoreaction in the $AlCl_3$-treated group. This was in the context of neuronal loss in AD as reported by Siracusa *et al.* (2020) and Yuceli *et al.* (2020). The strong positive ubiquitin immunoreaction and the appearance of large irregular plaques in the $AlCl_3$-treated group of the present work were in line with Nakamura (2018) and Watanabe *et al.* (2020), as well as in the context of AD pathology. Ubiquitin is a small regulatory protein directing the movement of important proteins and participating in both the synthesis of new proteins and the destruction of defective proteins (Gallo *et al.,* 2017 and Nakamura, 2018). They suggested that the ubiquitin system is involved in the development of inflammatory diseases implicated in neurodegenerative disorders. Being a part of the turnover system of protein, ubiquitin attaches to proteins forming ubiquitin conjugates, and tags them for disposal (Wilck *et al.*, 2017). In neurodegenerative disorders, ubiquitin conjugates contain disease-characteristic proteins such as amyloid, in AD. Accumulation of ubiquitin conjugates reflects the failed attempts by the ubiquitin system to remove these abnormal proteins. Moreover, a reduction in the activity of this system leads to the accumulation of proteins, and the mutations of those proteins cause more system failure (Mashahreh *et al.*, 2019). The morphometric findings of the present work came parallel with the histological and immunohistochemical results.

An improvement was observed in the present work after BM-MSCs therapy, and this improvement was at the histological, immunohistochemical and morphometrical levels. The stem cell-treated rats of the present work demonstrated a noticed clearance of the eosinophilic patches. This finding comes in accordance with that of Liu *et al.* (2020) and it is a good indicator of the recovery process. In the present study, neuronal proliferation was noticed. This improvement was in line with the assumptions of studies of Elia *et al.* (2019) and Liu *et al.* (2020). Andrzejewska *et al.* (2021) postulated that stem cells are capable of self-renewal, proliferation, differentiation and transformation into different types of central nervous system neurons and glial cells. Added to that, stem cells secrete neurotrophic factors providing a protective environment for endogenous cells (Liu *et al.,* 2020). These factors not only stimulate the differentiation of the resident stem cells but protect the regenerated neurons against stress-induced apoptosis (Han *et al.*, 2019B and Ramalingam *et al.,* 2021). Added to that, the immunomodulatory properties of MSCs could play a role in the inhibition of microglial activation, the mediator of neuroinflammation, by secreting many immunosuppressive cytokines (Gao *et al.,* 2016 and Rodríguez-Vera *et al.*, 2022).

CONCLUSION:

Aluminium chloride is an Alzheimerogenic chemical that causes hippocampal histological, immune-histochemical and morphometrical deterioration. MSCs could ameliorate these effects.

Declarations:

Ethical Approval: This study was carried out in strict accordance with the International Guidelines for the Care and Use of Laboratory Animals. The experimental protocol was approved by the Ethics Committee at the Faculty of Medicine, Assiut University, (Approval number: IRB17200423).

Conflict of Interest: The authors declare no conflicts of interest.

Authors Contributions: I hereby verify that all authors mentioned on the title page have made substantial contributions to the conception and design of the study. Mohamed N. Mahmoud proposed the research idea and methodology. Esraa K. Mohamed and Reneah R. Bushra conducted material preparation, data collecting, and statistical analysis.

Dorreia A. Mohamed and Reneah R. Bushra confirmed the accuracy and authenticity of the data and its interpretation, evaluated and thoroughly reviewed the manuscript, and approved the final article.

Funding: No funding was received.

Availability of Data and Materials: All datasets analysed and described during the present study are available from the corresponding author upon reasonable request.

Acknowledgements: Not applicable

REFERENCES

Abo-Azizaa F.; Zaki A. and Abo El-Maaty A. (2019): Bone marrow-derived mesenchymal stem cell (BM-MSC): A tool of cell therapy in hydatid experimentally infected rats. *Cell Regeneration;* 8:58-71.

Ali A.; Khalil M.; Abd El-latif D.; Okda T.; Abdelaziz A. and Abu-Elfotuh K.; et al. (2022): The influence of vinpocetine alone or in combination with Epigallocatechin-3- gallate, Coenzyme COQ10, Vitamin E and Selenium as a potential neuroprotective combination against aluminium-induced Alzheimer's disease in Wistar Albino Rats. *Archives of Gerontology and Geriatrics;* 98:104557.

Andrzejewska A.; Dabrowska S.; Lukomska B. and Janowski M. (2021): Mesenchymal stem cells for neurological disorders. *Journal of Advanced Research;* 8:2002944.

Beretta C.; Nikitidou E.; Streubel-Gallasch L.; Ingelsson M.; Sehlin D. and Erlandsson A. (2020): Extracellular vesicles from amyloid-β exposed cell cultures induce severe dysfunction in cortical neurons. *Scientific Reports;* 10(1):19656.

Birhane A.; Afwerk M.; Debeb Y. and Gebreslassie A. (2015): Review on histological and functional effect of aluminium chloride on cerebral cortex of the brain. *International Journal of Pharma Sciences and Research*; 6(8):1105-1116.

Cabianca D.; Muñoz-Jiménez C.; Kalck V.; Gaidatzis D.; Padeken J. and Seeber A.; et al. (2019): Active chromatin marks drive spatial sequestration of heterochromatin in C. elegans nuclei. *Nature;* 569:734-739.

Cattoretti G.; Pileri S.; Parravicini C.; Becker M.; Poggi S.; Bifulco C.; et al. (1993): Antigen unmasking on formalin-fixed, paraffin-embedded tissue sections. *The Journal of Pathology;* 171(2):83-98.

Choi S. and Tanzi R. (2019): Is Alzheimer's disease a neurogenesis disorder? *Cell Stem Cell*; 25:7-8.

Cosacak M.; Bhattarai P. and Kizil C. (2020): Alzheimer's disease, neural stem cells and neurogenesis: cellular phase at single-cell level. *Neural regeneration research;* 15 (5) : 824-827.

Da Mesquita S.; Ferreira A.; Sousa J.; Correia-Neves M.; Sousa N. and Marques F. (2016): Insights on the pathophysiology of Alzheimer's disease: the crosstalk between amyloid pathology, neuroinflammation and the peripheral immune system. *Neuroscience & Biobehavioral Reviews*; 68:547-562.

DeTure M. and Dickson D. (2019): The neuropathological diagnosis of Alzheimer's disease. *Molecular Neurodegeneration;* 14:32-50.

Dubois B.; Hampel H.; Feldman H.; Scheltens P.; Aisen P.; Andrieu S.; et al. (2016): Preclinical Alzheimer's disease: Definition, natural history, and diagnostic criteria. *Alzheimer's & Dementia;* 12(3):292-323.

Dudek S.; Alexander G. and Farris S. (2016): Rediscovering area

CA2: unique properties and functions. Nature reviews. *Neuroscience;* 17(2):89-102.

Dugger B. and Dickson D. (2017): Pathology of neurodegenerative diseases. *Cold Spring Harbor Perspectives in Biology*; 9(7): a028035.

Elia C.; Losurdo M.; Malosio M. and Coco S. (2019): Extracellular vesicles from mesenchymal stem cells exert pleiotropic effects on amyloid-β, inflammation, and regeneration: a spark of hope for alzheimer's disease from tiny structures. *BioEssays;* 41(4): e1800199.

El-Roghy E.; Soliman M.; Atteya, S.; Zakaria H. and Abdel Aziz S. (2022): Evaluation of Propolis supplementation on lung tissue toxicity induced by aluminum chloride in adult male albino rats: A histological and immunohistochemical study. *Egyptian Journal of Histology;* 45(4):1170-1188.

Elwakeel E. and Mohamed A. (2018): The Hepatotoxic effect induced by methotrexate therapy and protective role of bone marrow-derived mesenchymal stem cells in adult male albino rats. Histological and ultrastructural study. *Journal of American Science;* 14(5):1-28.

Gallo L.; Ko J. and Donoghue D. (2017): The importance of regulatory ubiquitination in cancer and metastasis. *Cell Cycle;* 16(7): 634-648.

Gao F.; Chiu S.; Motan D.; Zhang Z.; Chen L.; Ji H.; *et al.* (2016): Mesenchymal stem cells and immunomodulation: Current status and future prospects. *Cell Death and Disease*; 7: e2062.

Garcia-Leon J.; Vitorica J. and Gutierrez A. (2019): use of human pluripotent stem cell-derived cells for neurodegenerative disease modeling and drug screening platform. *Future medicinal chemistry;* 11(11): 1305-1322.

Goodarzi P.; Aghayan H.; Larijani B.; Soleimani M.; Reza Dehpour A.; Sahebjam M.; Ghaderi F. and Arjmand B. (2015): Stem cell-based approach for the treatment of Parkinson's disease. *The Medical Journal of the Islamic Republic of Iran*; 29:168-178.

Gugliandolo A.; Bramanti P. and Mazzon E. (2017): Mesenchymal stem cell therapy in Parkinson's disease animal models. *Current Research in Translational Medicine;* 65(2):51-60.

Han F.; Perrin R.; Wang Q.; Wang Y.; Perlmutter J.; John C.; *et al.* (2019B): Neuroinflammation and myelin status in Alzheimer's disease, Parkinson's disease, and normal aging brains: a small sample study. *Parkinsons Disease;* 2019: 7975407.

Han Y.; Li X.; Zhang Y.; Han Y.; Chang F. and Ding J. (2019A): Mesenchymal stem cells for regenerative medicine. *Cells;* 8(8):886-918.

Ju Y. and Tam K. (2022): Pathological mechanisms and therapeutic strategies for Alzheimer's disease. *Neural Regeneration Research;* 17(3):543-549.

Justin-Thenmozhi A.; Dhivya Bharathi M.; Kiruthika R.; Manivasagam T.; Borah A. and Essa M. (2018): Attenuation of aluminum chloride-induced neuroinflammation and caspase activation through the AKT/GSK-3β pathway by hesperidin in wistar rats. *Neurotoxicity Research;* 34(3): 463-476.

Kimberley D.; Andrea Z. and Robert H. (2017): Lipid processing in the brain: A key regulator of systemic metabolism. *Frontiers in Endocrinology*; 8:1-60.

Kizil C. and Bhattarai P. (2018): Is Alzheimer's also a stem cell disease? –The zebrafish perspective. *Frontiers in Cell and Developmental Biology;* 6:159.

Kumar V.; Weng Y.; Wu Y.; Huang Y. and Chou W. (2018): PKCε phosphorylation regulates the mitochondrial translocation of ATF2 in ischemia-induced neurodegeneration. *BMC Neuroscience;* 19(1):76-92.

Liddelow S.; Guttenplan K.; Clarke L.; Bennett F.; Bohlen C.; Schirmer L.; *et al.* (2017): Neurotoxic reactive astrocytes are induced by activated microglia. *Nature;* 541(7638):481-487.

Liu X.; Yang L. and Zhao L. (2020): Stem cell therapy for Alzheimer's disease. *World Journal of Stem Cells;* 12(8):787-802.

Lowe V.; Wiste H.; Senjem M.; Weigand S.; Therneau T.; Boeve B.; et al. (2020): Widespread brain tau and its association with ageing, Braak stage and Alzheimer's dementia. *Brain;* 141(1):271-287.

Mahdi O.; Baharuldin M.; Nor N.; Chiroma S.; Jagadeesan S. and Moklas M. (2019): Chemicals used for the induction of Alzheimer's disease-like cognitive dysfunctions in rodents. *Biomedical Research and Therapy*; 6(11):3460-3484.

Mahmoud M.; Zaghloul D.; Mohamed E. and Bushra R. (2024): The Possible Role of Bone Marrow Mesenchymal Stem Cells (BM-MSCs) in Ameliorating the Rotenone-Induced Changes on the Substantia Nigra in the Adult Male Albino Rat: Morphometric, Histological, and Immunohistochemical Study. *Egyptian Journal of Histology*; 47(1):436-448.

Mariacruz L. (2019): Regenerative medicine: could Parkinson's be the first neurodegenerative disease to be cured? *Future Science OA;* 5(9): FSO418.

Marzban M.; Mousavizadeh K.; Bakhshayesh M.; Vousooghi N.; Vakilzadeh G. and Torkaman-Boutorabi A. (2018): Effect of multiple intraperitoneal injections of human bone marrow mesenchymal stem cells on cuprizone model of multiple sclerosis. *The Iranian Biomedical Journal;* 22(5):312-321.

Mashahreh B.; Reiss Y.; Wiener R. and Ravid T. (2019): Methods in Enzymology. Chapter Four-Assays for dissecting the in vitro enzymatic activity of yeast Ubc7. *Academic Press*; 619:71-95.

Mazher K. and Hassan R. (2020): Histological, histochemical, and immunohistochemical studies of hippocampus in male New Zealand rabbits. *The Anatomical Record;* (1):1-7.

Nakamura N. (2018): Ubiquitin System. *International Journal of Molecular Sciences;* 19(4): 1080-1084.

Ramalingam M.; Jang S. and Jeong H. (2021): Neural-induced human adipose tissue-derived stem cells conditioned medium ameliorates rotenone-induced toxicity in SH-SY5Y cells. *International Journal of Molecular Sciences;* 22(5): 2322-2342.

Rodríguez-Vera D.; Abad-García A.; Vargas-Mendoza N.; Pinto-Almazán R.; Farfán-García E.; Morales-González J.; et al. (2022): Polyphenols as potential enhancers of stem cell therapy against neurodegeneration. *Neural Regeneration Research*; 17(10):2093-2101.

Saba K.; Rajnala N.; Veeraiah P.; Tiwari V.; Rana R.; Lakhotia S.; et al. (2017): Energetics of excitatory

and inhibitory neuro-transmission in aluminum chloride model of Alzheimer's disease: Reversal of behavioral and metabolic deficits by Rasa Sindoor. *Frontiers in Molecular Neuroscience;* 10: 323-338.

Sandip T. and Yogesh A. (2019): Neuroprotective effect of cardamom oil against aluminum induced neurotoxicity in rats. *Frontiers in Neurology;* 10:399-415.

Sengoku R. (2020): Aging and Alzheimer's disease pathology. *Neuropathology;* 40(1):22-29.

Singh A.; Bhardwaj V.; Ravi C.; Ramesh N.; Mandal A. and Khan Z. (2018): EGCG Nanoparticles attenuate aluminum chloride induced neurobehavioral deficits, beta amyloid and tau pathology in a rat model of Alzheimer's disease. *Frontiers in Aging Neuroscience;* 10:244-256.

Siracusa R.; Scuto M.; Fusco R.; Trovato A.; Ontario M.; Crea R.; *et al.* (2020): Anti-inflammatory and anti-oxidant activity of Hidrox in rotenone- induced Parkinson's disease in mice. *Antioxidants;* 9(9):824-842.

Song C.; Zhang Y.; Wu H.; Cao X.; Guo C.; Li Y.; et al. (2018): Stem cells: a promising candidate to treat neurological disorders. *Neural regeneration research;* 13(7):1294-1304.

Tietz T.; Lenzner A.; Kolbaum A.; Zellmer S.; Riebeling C.; Gürtler R.; *et al.* (2019): Aggregated aluminium exposure: risk assessment for the general population. *Archives of Toxicology;* 93:3503-3521.

Von Bartheld C.; Bahney J. and Herculano-Houzel S. (2016): The search for true numbers of neurons and glial cells in the human brain: a review of 150 years of cell counting. *The Journal of Comparative Neurology*; 524:3865-3895.

Watanabe Y.; Taguchi K. and Tanaka M. (2020): Ubiquitin, Autophagy and Neurodegenerative Diseases. *Cells;* 9(9):2022-2036.

Wilck N.; Fechner M.; Dan C.; Stangl V.; Stangl K. and Ludwig A. (2017): The effect of low-dose proteasome inhibition on pre-existing atherosclerosis in LDL receptor-deficient mice. *International Journal of Molecular Sciences;* 18(4):781-790.

Yuceli S.; Naz Yazici G.; Mammadov R.; Suleyman H.; Kaya M. and Ozdogan S. (2020): The effect of Rutin on experimental traumatic brain injury and edema in rats. *In Vivo;* 34(5): 2453-2460.

Zhang Z.; Buller B. and Chopp M. (2019): Exosomes beyond stem cells for restorative therapy in stroke and neurological injury. *Nature Reviews Neurology;* 15:193-203.